Review Article: Modern Trends in Imaging IX

Biophotonics techniques for structural and functional imaging, *in vivo*

Yasaman Ardeshirpour[a], Amir H. Gandjbakhche[a,*] and Laleh Najafizadeh[a,b]

[a]*Section on Functional and Analytical Biophotonics, Eunice Kennedy Shriver National Institute of Child Health and Human Development, National Institutes of Health, Bethesda, MD, USA*
[b]*Center for Neuroscience and Regenerative Medicine, Henry M. Jackson Foundation, Rockville, MD, USA*

Abstract. *In vivo* optical imaging is being conducted in a variety of medical applications, including optical breast cancer imaging, functional brain imaging, endoscopy, exercise medicine, and monitoring the photodynamic therapy and progress of neoadjuvant chemotherapy. In the past three decades, *in vivo* diffuse optical breast cancer imaging has shown promising results in cancer detection, and monitoring the progress of neoadjuvant chemotherapy. The use of near infrared spectroscopy for functional brain imaging has been growing rapidly. In fluorescence imaging, the difference between autofluorescence of cancer lesions compared to normal tissues were used in endoscopy to distinguish malignant lesions from normal tissue or inflammation and in determining the boarders of cancer lesions in surgery. Recent advances in drugs targeting specific tumor receptors, such as AntiBodies (MAB), has created a new demand for developing non-invasive *in vivo* imaging techniques for detection of cancer biomarkers, and for monitoring their down regulations during therapy. Targeted treatments, combined with new imaging techniques, are expected to potentially result in new imaging and treatment paradigms in cancer therapy. Similar approaches can potentially be applied for the characterization of other disease-related biomarkers. In this chapter, we provide a review of diffuse optical and fluorescence imaging techniques with their application in functional brain imaging and cancer diagnosis.

Keywords: Diffuse optical imaging, near infrared spectroscopy, functional brain imaging, fluorescence imaging, targeted fluorescent probe, Affibody, cancer treatment, cancer diagnostics, human epidermal growth factor receptor 2

1. Introduction

The first medical application of diffuse optics, proposed in 1929, was in the detection of breast cancer [1]. The method, called diaphanography, used the shadow of visible light transmitted through breast tissue to identify the location of a tumor. At the time, due to the low penetration of visible light and high scattering properties of breast tissue, the technique was not successful and subsequently it was disregarded.

In 1977, an article by Jobsis [2] opened an opportunity for *in vivo* optical imaging of the tissue. In his paper, Jobsis showed that tissue has negligible absorption properties in the near-infrared (NIR) spectrum, permitting the photons to penetrate deeply into the tissue. This discovery together with the advancements in theoretical physics and mathematical modeling of light penetration in the tissue [3], gave the progress in the in- *vivo* optical imaging research an exponential growth. In addition, significant improvements on the instrumental side (lasers, detectors, and hardware) further have facilitated the development of new spectroscopic and tomographic techniques.

In vivo optical imaging has been applied in different fields of medicine, including optical breast cancer imaging, functional brain imaging, cancer surgery, bone and joint imaging, and monitoring the photodynamic therapy and progress of neoadjuvant chemotherapy.

*Corresponding author: Amir H. Gandjbakhche, Section on Functional and Analytical Biophotonics, Eunice Kennedy Shriver National Institute of Child Health and Human Development, National Institutes of Health, Bethesda, MD, USA. E-mail: gandjbaa@mail.nih.gov.

In this Chapter, we will provide a general overview of existing *in-vivo* optical imaging techniques. In Section 1, the theory behind diffuse optical imaging is introduced, different reconstruction algorithms are briefly discussed, and techniques being employed to implement diffuse optical imaging instruments are reviewed. In Section 2, a brief discussion on applications of diffused optical tomography in cancer detection and monitoring the treatment has been provided. As a widely used application of diffuse optical imaging, functional brain imaging is discussed in Section 3. It will be shown how diffuse optical imaging has been used to capture both the brain's hemodynamic and neuronal responses. Section 4 introduces the diffused fluorescence imaging and its application in cancer diagnostics and treatment.

2. Diffuse optical imaging

The use of diffuse light in the near infrared (NIR) range for non-invasive imaging has been growing rapidly over the past three decades. The technique, going variously by the names of near-infrared spectroscopy (NIRS), diffuse optical topography, diffuse optical tomography, or near-infrared imaging (NIRI), follows the general concept of shining light onto the tissue, detecting it as it exits, and by using the absorption spectra of the underlying light-absorbing chromophores, estimating the changes in their concentrations [4].

In the NIR spectrum, the main endogenous contrast agents in the tissue are oxygenated hemoglobin (HbO), deoxygenated hemoglobin (HbR), water, lipid, melanin, myoglobin and cytochrome oxidase [5, 6]. Figure 1 shows the absorption spectrum of oxy- and deoxy-hemoglobin, water, and lipid in the tissue in the NIR window.

HbO and HbR are indicators of blood volume and oxygenation, (the sum of HbO and HbR makes up the total hemoglobin (HbT) and is a good estimator for the blood volume), whereas the cytochrome enzymes are markers of intracellular energy [8, 9]. Since the absorption coefficient of tissue chromophores are negligible in the NIR region, light can penetrate deeply (a few centimeters) into tissue. At wavelengths lower than 650 nm, absorption by hemoglobin limits the penetration of photons into tissue, while at wavelengths higher than 900 nm, absorption by water dominates. Diffuse optical imaging techniques take advantage of these
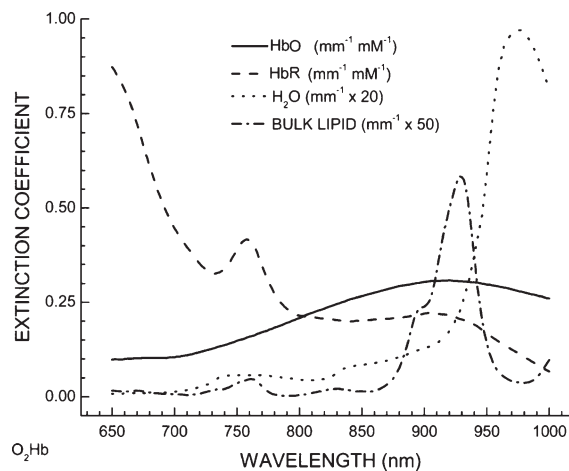

Fig. 1. Absorption spectrum of main chromophores in tissue in the NIR window (after [7]).

differences and produce spatially resolved images that may present the specific absorption and scattering properties of the tissue, or physiological parameters such as blood volume and oxygenation [8]. However, due to the high scattering properties of the tissue media, the resolution can be as low as a few millimeters to a centimeter based on the wavelength of the light, tissue type, and depth of the imaging plane.

Diffuse optical imaging techniques can be categorized into two major groups: those which provide topographic measurements (diffuse optical topography), and those which create 3-D tomographic images (diffuse optical tomography) [10]. In what follows, a brief review of the two techniques is provided, followed by a description of the available techniques for developing diffuse optical imaging instruments.

2.1. Diffuse optical topography

Optical topography has been commonly used to monitor functionality of the brain in the cortical region. Diffuse optical topography can be conducted in two ways: direct topography or near infrared spectroscopy, and reconstructed topography [10].

Near infrared spectroscopy is the most practiced approach of diffuse optical topography. In this technique, a spatially distributed array of light sources and detectors will be placed on the surface of the object of interest, for example subject's head. Due to scattering properties of the tissue, near infrared photons scatter through the tissue, and a small fraction of them will reach the detector, sampling a diffuse volume

between the two positions [11]. If the optical properties of the tissue changes over time (for example, if changes occur in the concentration of its light absorbing chromophores) the probability of a photon reaching the same detector, and therefore, the detectable intensity, will alter. These changes measured between each source-detector pair, can be used to construct a 2-D topographical map [10].

Reconstructed topography technique, by creating a depth-resolved image of the measured absorption changes, attempts to reconstruct the data on a 3-D image [10]. This is generally done through finding a correct absorption distribution by matching the measured data with simulation results of several absorption distributions within the 3-D image [12–14]. Therefore, it becomes necessary to record signals at several source-detector distances, as for each measurement, there should be only one absorption distribution and depth-resolved information can be extracted. Modeling of light propagation is usually done through Monte Carlo simulations, or diffusion approximation to the radiative transport equation. A more complete discussion is provided in [10].

2.2. Diffuse optical tomography

Diffuse optical tomography uses an approach similar to x-ray computed tomography to reconstruct 3-D images of absorption and scattering coefficients of the tissue. Similar to reconstructed topography, optical tomography requires recording of a series of measurements through the tissue, but in this case, the number of necessary measurements for constructing a 3-D image are larger and they also need to be obtained at different angles [10]. The primary difficulty of diffuse optical tomography is related to the fact that multiple-scattering dominates NIR light propagation in tissue, making 3D localization of lesions and accurate quantification of its optical properties difficult and undetermined. For brain imaging, the technique requires the head to be surrounded by an array of light sources and detectors, and until now, due to high attenuation in adult heads that prevents light from penetrating through the deeper brain regions, optical tomography has only been used to study the brain functionality in infants [15].

The image reconstruction can be improved using a second modality, e.g. ultrasound, x-ray or Magnetic Resonance Imaging (MRI), to confine the target region [16–20]. In the last three decades many imaging algo-

rithms based on analytical, numerical or statistical models have been developed. The fastest algorithms are based on analytical approximation of diffusion equations [21, 22]. Algorithms in a second category are developed based on the numerical models of diffusion equation or photon transport model. These solutions are more computationally expensive, but are capable of modeling any arbitrary geometry and boundary conditions. The finite element method [13, 23], boundary element method [24], and finite difference method [25] all fall in this category. The third category is based on statistical modeling, e.g. the monte-carlo simulation and random walk theory [26]. These algorithms track and record the path of each photon in turbid media individually. They provide the most accurate results; however, they are also computationally expensive and time consuming. In general, the quality of reconstructed image depends upon many parameters, including signal-to-noise ratio, measurement geometry, and depth of the target (for example lesion) from the optical probe [27]. A more thorough review of optical tomography is provided in [10, 21, 22, 28].

2.3. Diffuse optical imaging instruments

Three essential components exist in any diffuse optical imaging system: a NIR light source, a detector, and required electronics for the two [4]. The commonly used options for the light source are laser diodes and light emitting diodes (LEDs), with the laser diodes capable of providing a larger light power. As for the detectors, the choice of the detector for a given application depends on the desired sensitivity, stability and dynamic range, as well as more practical concerns such as size and cost [8]. Avalanche photodiodes (APDs) are the most commonly used ones, due to their low cost, fast acquisition rate and relatively high light detection sensitivity. Silicon photodiodes have been also used; however they have lower sensitivity than APDs. In multi-wavelength spectroscopic measurements, charge-coupled devices (CCDs) are generally used which have the ability to detect multiple wavelengths simultaneously. A comprehensive review of detectors can be found in [29]. Finally, electronic components are required to drive the light sources and to do demultiplexing the original signals from multiple measurement points.

In terms of measurement schemes, optical diffuse imaging instruments can be classified into three different categories: continuous-wave (CW) systems,

frequency domain (FD) systems, and time domain (TD) systems. The most commonly used one is the CW system, in which the light is emitted continuously with constant amplitude, or modulated at low frequencies (a few kHz) to enable separation following detection. CW systems only measure the attenuation in the amplitude of the incident light, and therefore, are not able to provide information on absorption and scattering, separately [9, 30]. To overcome this limitation, different approaches like multi-spectral method [31] or spatial frequency method [32] have been used to improve CW reconstruction. Multispectral imaging improvement is based on the fact that tissue chromophore concentrations and Mie scattering coefficients are wavelength independent [31]. Therefore, these parameters can be reconstructed simultaneously from measurements at different wavelengths by considering their a-priori spectral properties. The spatial modulation method uses an illumination light with a spatial sinusoidal modulation pattern. Since the spatial modulation transfer function of a turbid medium has both the information of depth and the optical property of the media, it can help to improve quantitatively the reconstructed absorption and scattering values of the turbid media [32, 33]. Probably, CW optical diffuse imaging technique has found its most application in optical topography of the brain cortex [8]. By maintaining small source-detector separation, changes in the hemodynamic responses within tens of milliseconds can be captured. Several CW systems each offering their own specifications, have been developed for this application. By employing solutions, such as back-projection algorithms [34], advanced versions of the CW systems have been also developed for optical tomography of brain (DYNOT) or breast (Phillips).

TD instruments use femtosecond or picosecond laser pulses that are fired sequentially, to measure the temporal distribution of photons, known as temporal point spread function (TPSF), as they exit the tissue. The detector should have a very fast time response and can be implemented by a time-gated intensified charge coupled device (ICCD) or a fast photomultiplier tube (PMT) with a time-correlated single photon counter (TCSPC). The delay and shape of this distribution is then used to extract information about tissue's absorption and scattering properties [35]. TD systems generally employ either a *transillumination* technique, in which source and detectors are placed on opposite sides of the tissue, or a tomographic technique,

which enables sampling multiple lines-of-sight across the entire volume [8].

In the frequency domain technique, the light source is sinusoidally modulated at frequencies in the range of 10 s to 100 s of MHz. Passing modulated light through tissue changes the amplitude and phase of the transmitted and/or reflected signal [36]. In fact, FD systems can be linked to the TD systems via the Fourier transform [37], and both the transillumination and tomographic approaches, described above, are applicable for the FD systems as well [8].

Each of these techniques has their own advantages and disadvantages. CW systems are the least expensive option among three, however, they fail to provide separate quantitative information about the tissue's scattering and absorption properties. In addition, due to the characteristic 'banana' shape of photon measurement density function (PMDF) intensity measurements in these systems are not uniformly sensitive to the tissue's optical properties (more sensitive at or immediately below the surface than deeper within the tissue) [21, 22]. TD systems are the most complex ones and are generally slow, however they can obtain the highest spatial resolution [9] while providing detailed information about both absorption and scattering. FD systems are capable of achieving higher temporal resolution than TD systems, and are less expensive, however, their sensitivity reduces if the thickness is larger than 6 cm [8].

3. Diffuse optical imaging of cancer

Tumor cells, in order to grow beyond 1 to 2 cubic millimeters, require effective interaction with the blood vessels to obtain oxygen and nutrients and get rid of metabolic waste products and carbon dioxide. Therefore, one of the main requirements for cancer cells to survive and grow is the formation of a new network of blood vessels, which is called angiogenesis. Total hemoglobin concentration and oxygen saturation of the lesion are correlated highly with tumor malignancy. In general, the physiological difference between cancer lesion and normal tissue influences their optical signature (optical absorption and scattering parameters and refractive index). In the last three decades many efforts has been done to detect these differences, specifically in breast cancer patients, by diffuse optical tomography method.

Figure 2 shows the difference between the scattering and absorption spectrum of malignant and normal
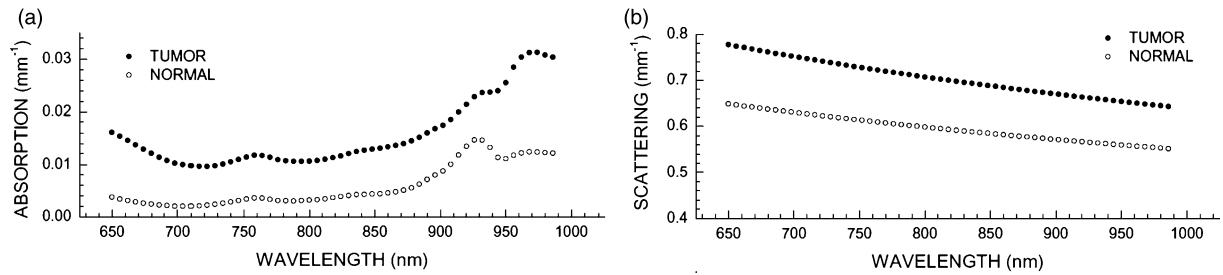
Fig. 2. Absorption (a) and scattering (b) spectrum of tumor vs. normal breast tissue (after [7]).

breast tissue in near infrared spectrum [7]. The data shows higher hemoglobin absorption (both oxy- and deoxy) in tumor lesion relative to normal tissue, because of the occurrence of angiogenesis. In tumor tissue, higher absorption around 980 nm is due to greater water volume inside the tumor. There is also a spectral broadening and shifting in this region that is probably due to the different type of chemical binding of the water molecules in tumor tissue compared to normal tissue. Another difference is in the distinctive peak at 930 nm wavelength which is associated to lipid. The lipid concentration in tumor is usually lower than in normal tissue. The scattering enhancement observed in cancer tissues might be related to the changes in cell nuclear size and increase of the concentration of cell organelles such as mitochondria [38].

One of the promising applications of diffuse optical imaging is in monitoring of effectiveness of treatment in cancer patients. Recent studies have shown diffuse optical imaging can be used to monitor the therapeutic response of the patients during the neoadjuvant chemotherapy. Neoadjuvant chemotherapy is a pre-operative chemotherapy in patients with advanced breast cancer. Several clinical studies showed that if a patient responds well to neoadjuvant chemotherapy, a decrease in size and angiogenesis of the primary tumor can be detected by diffuse optical imaging [39, 40].

Co-registration of diffuse optical imaging with high resolution imaging modalities, such as MRI, US and CT can provide functional information within the framework of anatomical structures.

To improve the contrast between tumor and normal tissues, exogenous contrast agents like indocyanine green (ICG) have been used in the past [41]. Due to the leakiness of the tumor vascularization, small dye molecules with a high absorption coefficient in NIR region, can accumulate in the tumor area longer than

normal tissue and can improve the contrast between tumor region and the surrounding normal tissue.

4. Optical imaging of brain function

The application of optical diffuse imaging for non-invasive monitoring of brain function has experienced exponential growth in recent years. NIR has been successfully demonstrated to detect hemodynamic, metabolic, and neuronal signals associated with brain activity. In this section, we review how diffuse optical imaging is being used for monitoring the brain functionality.

4.1. Cerebral cortex

Since the penetration depth of light into tissue is limited, majority of the brain studies employing light
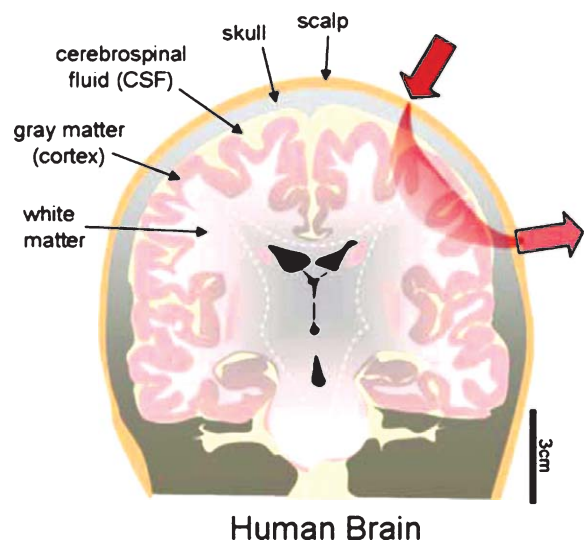

Fig. 3. Human brain and placement of optodes (after [42]).

have focused on the functionality of the cerebral cortex. In optical imaging of the brain, light sources and detectors are placed over the head (Fig. 3). The light emitted from the source into the brain must pass through superficial layers with low absorption property in the near infrared region, before reaching the brain tissue. These layers include the scalp, the skull, meninges, and the cerebrospinal fluid (CSF).

The cerebral cortex, being the largest part of the brain, represents a highly-developed structure responsible for high-level brain activities. The frontal lobe is responsible mainly for cognitive functions including problem solving, planning and making decision, judgment and memory. The functionality of parietal lobe includes sensation of pain and touch and reception and processing of sensory information from the body. The occipital lobe, located at the tail end part of the cerebral cortex is responsible for vision. Finally, the temporal lobe is mainly involved in hearing and language processing.

To date, a large number of optical brain imaging studies have been conducted which have successfully captured functionality of the cerebral cortex in response to cognitive stimulations [43–51], visual stimulations [52–60], motor and sensorimotor stimulations [61–69], and also language-related studies [70–76].

4.2. Slow signal: Hemodynamic response

When activation occurs in a specific region of brain, each individual local nerve cell produces electrical signal which is transmitted through its axons and dendrites to the neighboring cells. This neuronal activity requires consumption of energy and therefore, a rise in regional cerebral blood flow and cerebral blood volume would follow to supply the increased demand for glucose and oxygen. The major oxygen carrier in blood, is hemoglobin, and as a result, activation in brain would cause an increase in local HbO concentration and a decrease in HbR concentration [77, 78]. This activation-induced regional vascular change is known as the hemodynamic response [79]. It starts to rise with a short delay of 1-2 seconds after stimulus onset, and reaches to a peak over 4–6 seconds before slowly decreasing to the baseline level [11]. Typically, an undershoot below baseline at roughly 10 second post-stimulus is observed before the vascular physiology returns to the baseline level. Since the changes in the hemodynamic response are in the seconds range

(compared to mili-second rang of neuronal response), the hemodynamic response occasionally is referred to as slow signal.

The activation-induced regional decrease in the local concentration of HbR corresponds to the blood-oxygen level dependent (BOLD) signal that is used in functional MRI. Diffuse optical imaging, being sensitive to both HbR and HbO chromophores is capable of measuring the changes in the concentrations of both HbR and HbO. In what follows, we will review the techniques that are being used to obtain estimates of changes in the two chromophore concentrations during functional brain activation.

4.2.1. Modified beer lambert law

The modified Beer Lambert Law (MBLL), expressed in equation (1), is the most widely used model for calculating the activation-induced changes in the concentrations of HbR and HbO.

$$OD = -\log\left(\frac{1}{I_0}\right) = \mu_a(\lambda)DPF(\lambda) + G(\lambda) \quad (1)$$

In (1), OD is the optical density, I_0 is the incident light intensity, I is the detected light intensity, λ is the wavelength, $DPF(\lambda)$ is the mean pathlength traveled through the tissue, $G(\lambda)$ is a geometry-dependent factor, and $\mu_a(\lambda)$ is the absorption coefficient of tissue defined as

$$\mu_a = \sum_n \xi_n(\lambda)C_n \quad (2)$$

where n is the number of chromophores, $\xi_n(\lambda)$ is the specific absorption coefficient of a particular chromophore, and C_n is its concentration [10]. Since the value of $G(\lambda)$ in (1) is difficult to determine, it is common to obtain the *changes* in chromophore concentrations with respect to a reference stage. To obtain the quantification changes in concentrations of both HbO and HbR, two wavelengths would be required. In this case, by knowing the absorption coefficients at each wavelength, and applying the MBLL, we can find the concentration changes of HbR (ΔC_{HbR}) and HbO (ΔC_{HbO}) as

$$\begin{bmatrix} \Delta C_{HbO} \\ \Delta C_{HbR} \end{bmatrix} = \begin{bmatrix} DPF_{\lambda 1}\xi_{HbO_{\lambda 1}} & DPF_{\lambda 1}\xi_{HbR_{\lambda 1}} \\ DPF_{\lambda 2}\xi_{HbO_{\lambda 2}} & DPF_{\lambda 2}\xi_{HbR_{\lambda 2}} \end{bmatrix}^{-1} \begin{bmatrix} \Delta OD_{\lambda 1} \\ \Delta OD_{\lambda 2} \end{bmatrix} \quad (3)$$

Although MBLL provides a simplified model for a good estimation of the concentration changes of chromophores in highly scattering media with uniform properties, it comes with some limitations. For example, the homogenous assumption is not valid in most biological mediums. In addition, *DPF* is wavelength dependent, and its accurate estimation is difficult, which can result in incorrect calculation of HbO and HbR concentration changes [80]. Also, since HbO and HbR changes are not generally uniformly distributed, partial volume scaling needs to be taken into account [81]. Furthermore, MBLL does not provide a framework for image reconstruction [9]. To combat these limitations, other techniques employing diffusion approximation to the radiative transport equation have been used.

4.2.2. Photon diffusion equation

The photon diffusion approximation, which accurately models the migration of photons in a scatter dominant medium, is expressed as [82–84]:

$$-D\nabla^2\Phi(r, t) + \upsilon\mu_a\Phi(r, t) + \frac{\partial\Phi(r, t)}{\partial t}$$
$$= \upsilon S(r, t) \qquad (4)$$

In (4), $\Phi(r, t)$ is the photon fluence at position r and time t, υ is the speed of light in the medium, D is the diffusion coefficient ($D = \upsilon/\mu_s'$, where μ_s' is reduced scattering coefficient), and $S(r, t)$ is the source distribution of photons [9]. For simple semi-infinite mediums, analytical solutions to equation (4) exist [9]. Also, Rytov and first-order Born approximations have been used to find the solution to (4) [85]. For more complex situations, techniques such as finite element methods and Monte Carlo modeling have been applied to simulate light propagation in the head [10].

4.2.3. Sources of noise and noise removal techniques

Functional brain imaging using diffuse optical imaging techniques have been gaining more and more attention in recent years; however, similar to other imaging techniques, the recorded data is not immune to the influence of noise which is introduced from a variety of sources. If noise-induced signal changes are not identified and further removed from the measurements, incorrect conclusions could be made for the corresponding functional activations.

Noise influencing the optical data can be categorized in three distinct groups [81]: instrumental noise, experimental errors, and physiological artifacts. Examples of instrumental noise include electronic noise such as Johnson-Nyquist or Shot noise, coming from a computer or other electronic hardware, or low-frequency drift which may be due to small instabilities in the laser diode light sources [86]. Such instrumental noise components mostly can be separated from the data through appropriate filtering.

Sources for experimental errors could be subject movement, or noncompliance with the stimulus paradigm [81]. Although if the optical probes are well secured to subject's head, NIRS becomes more tolerant to subject's movement. This feature has been used to study brain functionality during mobility [87]. However, in some cases, presence of motion artifacts in the measured signal is inevitable. Several signal processing techniques, including adaptive filtering, regression, Wiener filtering, principal component analysis, independent component analysis, and wavelet analysis, have been applied for the removal of motion artifacts [88–92]. The use of redundant imaging channel with a negligible source-detector separation for identification of motion artifacts has also been investigated [86]. The work in [86] also suggests that independent component analysis and regression could be the most effective signal processing technique for removing motion artifacts.

Since the diffuse light travels through the superficial layers before it gets to the detector, there will also be interference in the recorded signal from the physiology fluctuations present in the superficial layers. These fluctuations, which form the dominant source of noise, include cardiac pulsation, respiratory signals, systematic blood pressure, and Mayer waves [4, 81, 86, 93, 94]. To eliminate the influence of physiological noise, signal processing techniques based on approximate frequency content of the signal, or the spatial covariance of physiology are generally used [81]. Cardiac pulsation has a frequency component around 1 Hz, and blood pressure oscillations are generally found between 0.08–0.12 Hz. Therefore, bandpass filters can be used to reduce the contributions of these high/low frequency components. However the selection of frequency cut offs should be done carefully to avoid removing the frequency components associated with the hemodynamic signal [81]. Principal component analysis techniques taking advantage of spatial covariance properties of physiological signals

have also been successfully used for the removal of physiological noise [94].

4.3. Fast signal: Neuronal response

While the majority of works related to optical imaging of the brain have been concentrated on capturing the slow hemodynamic response, several attempts have also been made to optically measure the neuronal activities [35, 95–107]. The idea of noninvasively measuring this evoked fast optical signal can be traced back to [108], in which it was demonstrated that neuronal activity potentially results in light scatter changes. These scattering changes, occurring on a time scale considerably faster than the hemodynamic response, are believed to be related to changes in the ion currents across the neural membrane during neuronal activity that somehow alters neural tissue's optical properties [103].

The main challenge in detecting fast optical signal is its very low signal to noise ratio (SNR). Several techniques have been made to overcome this problem. Adaptive filtering and independent component analysis were used in [105] and finger tapping related neuronal signals were captured in 9 out of 14 subject. Other approaches used to maximize the SNR include employing high power emitting sources and photomultiplier tube detectors [95], using multiple source-detector pairs [102], or special π-sensors [107], and averaging across large number of trials. Majority of these works have used FD instruments. Recently, the work in [103] used a CW system, and applied ICA to reduce the global interface (contributions from superficial layers and the heartbeat), and then averaging techniques for signal processing, and was able to detect the event related potentials related to a visual oddball task in majority of subjects.

Although there are controversial results regarding the capabilities of diffuse optical imaging instruments to record neuronal activities, the majority of published work so far provide a strong support that fast optical signal can be measured [98].

4.4. Comparison with other functional brain imaging techniques

Here we provide a comparison among existing brain imaging techniques in terms of their spatial and temporal resolutions (Fig. 4). Electroencephalography
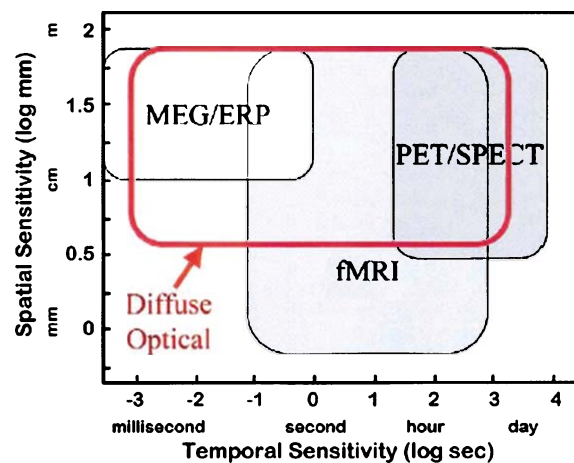

Fig. 4. Comparison of different imaging modalities in terms of their spatial and temporal sensitivities (after [4]).

(EEG), and Magnetoencephalography (MEG) directly measure the neuronal activity and therefore, provide a strong temporal sensitivity. However, they have limited spatial resolution. Imaging modalities such as functional MRI (fMRI), PET, and SPECT offer high spatial resolution, but cannot provide millisecond temporal resolution as EEG and MEG do.

Diffuse optical Imaging methods offer excellent temporal sensitivity in conjunction to providing reasonable spatial sensitivity [4]. As it was mentioned studies exist that have used NIRS to capture event related optical signal corresponding to neuronal activity. In addition, compared to PET and fMRI, the NIRS instruments can be made portable. NIRS is also a noninvasive technique without requiring radioactive compound (which are needed in PET), and has been used in many functional brain imaging studies of neonates and children.

5. Fluorescence imaging

Another *in-vivo* diffuse optical method is fluorescence imaging which can be used to detect either the native (endogenous) tissue fluorophores (autofluorescence) [109] or the exogenous fluorescent probes [110]. In this section, brief description of fluorescence imaging systems is provided, followed by a discussion on fluorescent probes. In the last part, computational algorithms and the information that can be extracted through them were discussed and several examples were provided.

5.1. Fluorescent imaging systems

Similar to diffuse optical imaging, fluorescence imaging systems can be categorized to CW, FD and TD systems.

5.1.1. Fluorescence intensity imaging (CW)

The most common fluorescence imaging technique is continuous wave (CW) fluorescence imaging. This method uses a CW or very low frequency modulated light source to provide the excitation light. The intensity of the reflected or transmitted fluorescence signal is detected by a CCD camera or PMT. Implementation of this method is less expensive and easier than other fluorescence imaging techniques that we will discuss later. The disadvantage of this method is that it only captures the intensity information of the fluorescence signals. Therefore, this approach is sensitive to the fluctuations of the excitation light, distance of the probe from the tumor, and parameters of the system.

The optical signal can be detected through transillumination and/or epi-illumination of the tissue. In transillumination, the source and detector are placed on opposite sides of the tissue; and the detector captures the photons that transmitted through the tissue. In epi-illumination the source and detectors are placed on the same site of the tissue and the reflected fluorescence signal from the tissue is detected by the detector. In many medical applications, using transillumination is not possible and the source and detectors have to be placed on the same site. Owing to the diffusion of excitation and emission light in tissue, epi-illumination can image fluorescence activities at depths ranging from millimeters to a few centimeters, based on the excitation and emission wavelengths of the fluorophore.

One of the methods that can help to reduce uncertainties in the analysis of raw CW fluorescence imaging, and improve its quantitative value, is normalization of the fluorescence intensity to the background signal. This approach decreases the sensitivity of the fluorescence signal to the system parameters, such as intensity of excitation light and gain of the detector modules, as well as background tissue properties. It has been shown that data analysis for fluorophores, deeply embedded in tissue and highly heterogeneous media works better, if the normalized ratio of fluorescence emission signal to the unfiltered diffused signal, coming from the excitation light, is used instead of the ratio of fluorescence to background signal [111, 112]. The main reason is that

the unfiltered diffused signal contains more information about the heterogeneity and optical properties of the background tissues than just the background fluorescence signal, when measured before injection of the fluorescence dye.

The same as diffused optics, one of the challenges of fluorescence imaging in deep tissue imaging is the high scattering properties of the tissue. Tissue scattering reduces the resolution of the optical imaging significantly. Same a diffused optical tomography, co-registration of fluorescence imaging with high resolution imaging modalities, such as CT, MRI, and US can provide functional information within the framework of anatomical structures [113–121]. In deep tissue imaging, the absorption and scattering of properties of the tissue have a big impact on the detected fluorescence intensity and lifetime and has to be considered in the imaging reconstruction algorithms. The absorption and scattering properties of the tissue can be obtained by diffuse optical tomography (DOT) methods [122]. In fluorescence tomography, anatomical structures can help to decrease the unknown variables in the fluorescence reconstruction algorithms and improve the 2D and 3D images of the fluorescent probes [18, 123].

5.1.2. Fluorescence lifetime imaging (frequency domain, time domain)

Fluorescence lifetime imaging is based on the average time that excited fluorophore stays in the excitation state before its transition to the ground state accompanied by emission of a photon. Fluorescence lifetime can be measured either by time-domain or frequency domain techniques. In the frequency domain technique, the excitation light intensity is sinusoidally modulated at 100 s of MHz. Passing modulated light through tissue changes the amplitude and phase of the fluorescence signal. Fluorophores with larger lifetimes have longer phase shifts and amplitude attenuation.

In the time domain system, a very short laser pulse (sub-nsec) illuminates the target. The detector has a very fast time response and can be implemented by a time-gated ICCD or a fast PMT with a time-correlated single photon counter (TCSPC). Figure 5 shows the schematic of the fluorescence small animal imager consisting of a CW and a time domain fluorescence system that was developed by our group.

A cooled, charge-coupled device (CCD) camera was used in CW mode with a bandpass filter (800 nm ± 20 nm) to find the location of the tumor
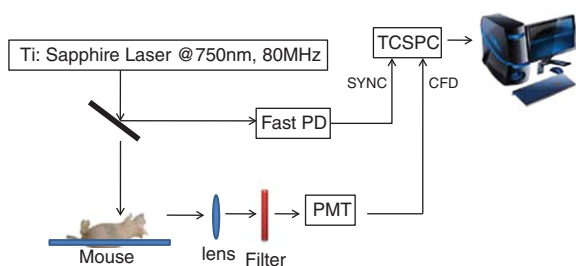
Fig. 5. Schematic of our time-resolved small animal imaging system.

(ROI) and position the scanner of the time domain system to the ROI. The same camera was used without the filter to capture the white light image of the small animal. The field of view of the CCD camera was $12 \times 12\,cm^2$. The time domain system consisted of a tunable Ti-Sapphire Pulse Laser with a pulse width of 100 fs and repetition rate of 80 MHz (Tsunami, Spectra Physics, Mountain View, CA). The laser peak was set at excitation wavelength of 750 nm. The femto-second laser pulse scanned the target (tumor or contralateral site) of the animal in a raster pattern through a scanning head with the source and detector fibers at 2 mm distance. The scanner was programmed to scan any area in the field of view of the CCD camera. The integration time for each pixel was selected based on the maximum intensity of the detected fluorescence signal and the saturation point of the PMT. The reflected fluorescence signal was filtered by a high-pass emission filter at 780 nm and was detected by a photomultiplier tube (R7422, Hamamatsu Corporation, Hamamatsu City, Japan). Detected photons were counted by a time-correlated single-photon counter (SPC-730, Becker & Hickl, Berlin, Germany). Initialization, scanning, and acquisition were controlled by the Labview software. The animal was placed within a dark chamber on a temperature-controlled scanning stage and was anesthetized through a nose cone [124].

As with CW fluorescence imaging, *in vivo* lifetime imaging can be implemented with transillumination, epi-illlumination, and fluorescence tomography [125–128]. Limitations of both the time domain and frequency domain techniques are similar to those discussed in the previous section on CW intensity fluorescence imaging technique.

In comparing the time and frequency domain techniques, it should be noted that, in practice, implementation of the frequency domain is usually limited to one or a few modulation frequencies; the time domain data can provide more information about the probed media, since a short laser pulse contains a much broader range of the modulation frequencies, including the zero-frequency component. The effect of measurement noise is less in the time domain method, since its lifetime calculation is based on the slope of the detected signal and the slope of a signal is less susceptible to noise than its amplitude [129]. On the other hand, instrumentation for time-resolved imaging is considerably more expensive and data collection time is longer relative to a frequency domain system. Therefore, to calculate the lifetime in applications that need very fast imaging, the frequency domain method is more suitable.

Fluorescence lifetime can provide useful clinical information, because fluorescence lifetime is potentially sensitive to local biochemical environment, e.g. temperature and pH, or molecular interactions [130, 131]. On the other hand, its value does not depend on the concentration of the fluorophores or the intensity of the excitation light (before saturation) [132]. The sensitivity lifetime to these parameters is based on the structure of the dye. Therefore, to evaluate specific properties of the probe environment in tissue, it is important to choose a proper dye with lifetime sensitivity mainly to one specific factor.

Lifetime imaging has been used extensively in cell biology and in *in vitro* studies. It has also been applied to endogenous and exogenous fluorophores in both *ex vivo* tissue and *in vivo* animal studies [124, 131]. Fluorescence lifetime imaging has not been conducted with exogenous contrast agents in clinical studies due to the lack of FDA-approved exogenous contrast agents, but some companies, e.g. Li-Cor Corp., have started pre-clinical/clinical studies to obtain FDA approval for their near infrared fluorescent dyes. Potential applications of *in vivo* fluorescence lifetime in cancer diagnosis and investigation of early-phase treatment response in the clinic are as follows: *in vivo* monitoring of environmental differences (e.g. pH) in the tumor compared to normal tissue [133–135]; *in vivo* monitoring of the internalization of a specific drug into malignant and disease cells by using a fluorescent probe with a pH-sensitive lifetime; developing a fluorescent probe that is sensitive to molecular interactions and capable of revealing the binding of a specific drug molecule to a specific disease/cancer receptor. It should be noted that lifetime imaging based on endogenous fluorophores has already been used in clinical studies of human skin [136].

5.2. Fluorescent probes

In general, fluorophores can be categorized in two groups of endogenous (intrinsic and native) fluorescent markers in the tissue or exogeneous (externally added) fluorescent dyes.

5.2.1. Endogenous fluorescent probes

In tissue, the most important endogenous fluorophores in the visible wavelengths are aminoacids, lipofuscins, melanin, collagen, elastin, nicotinamide adenine dinucleotide (NADH), and flavins [109, 137]. In the near-infrared part of the spectrum, even though the autofluorescence of the tissue is not significant, the most important endogenous fluorophore is porphyrin [138]. In general, cancer tissue shows different autofluorescence signal than the adjacent normal tissue; therefore, in many endoscopic systems, the fluorescence imaging has been added to the white field imaging system and is used to find the location of the lesion and/or determine its boundary during surgery [139–141].

5.2.2. Exogenous fluorescent probes

Exogenous fluorescent probes can provide optical images with better sensitivity and specificity compared with absorption and endogenous fluorophore images, and provides new information about tissue micro-environment, such as pH or hypoxia and help to categorize cancer type by distinguishing its different biomarkers [110, 142–145].

5.2.2.1. Non-targeted fluorescent probes: Non-targeted exogenous fluorescent contrast agents like ICG have been used to enhance the contrast of diffuse optics for tumor detection [146]. Accumulation of non-targeted fluorescent dye in the tumor is due to the leakiness of its vascularization which helps the dye to accumulate inside the tissue and delays its clearance time compared to the normal tissue.

Figure 6 shows higher tumor vascularization (angiogenesis) of the tumor compared with the contralateral site, imaged using AngioSense 750 (VisEn Medical, Inc. Bedford, MA). Anesthetized mice with N87 human xenograft, which is a tumor model with high HER2 expression, were injected intravenously with 150 μL of 2 nmol of AngioSense 750. The results show higher accumulation of Angiosense 750 fluorophores in the tumor area compared to contralateral site.
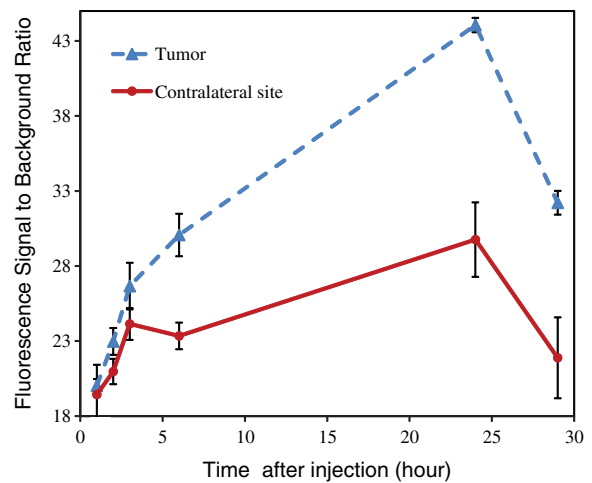

Fig. 6. Monitoring the uptake of AngioSense 750 at the tumor compared to the contralateral site (control) in three mice. The higher uptake at the tumor site indicates its higher vascularization. The fluorescence intensity at the tumor and contralateral sites was normalized to the background intensity of the tumor area before injection (after [147]).

5.2.2.2. Targeted fluorescent probes: A better option is if the fluorochrome conjugates to a ligand that can bind to a specific cancer receptor; it can stay longer inside the tumor and improves the signal to background ratio significantly [110, 142, 145].

On the other hand, efficacy of drugs targeting specific tumor receptors such as monoclonal antibodies (MAb), depends strongly on the expression of tumor-specific biomarkers. The main purpose of MAb drugs is to selectively target the cancer-causing biomarkers, inactivate specific molecular mechanisms responsible for cell malignancy, and deliver the toxin only to the malignant cells [148–150].

Recent advances in these drugs created a new demand for developing fluorescent probes that bind selectively to the cancer-causing biomarkers and also for developing non-invasive *in vivo* imaging techniques for detection of cancer biomarkers and monitoring their down regulations during treatment, especially, in the early stages of therapy.

Many criteria should be considered in these systems. They should be able to detect and quantify specific cancer biomarkers and monitor the interaction of a drug with cancer cells. To pursue this, more efficient and specific molecular imaging probes need to be designed to target biochemical and pathophysiological features of tumors. Molecular imaging probes should express a

minimum level of toxicity and side effects on normal tissue and organs. They should give enough contrast and signal to background ratio at low concentration levels (in the nanomolar to micromolar range). They should have a stable specific binding, high accumulation in the target region, and fast washout time from the blood and normal tissues. On the other side, the clearance of the probes from the body has to be slow enough to allow accumulation in the target sites and obtain a good affinity and binding to the receptors. It is also important that if these imaging probes are being used to monitor therapy that they do not interfere with a drug's functionality [151, 152].

Each targeted molecular probe usually consists of three parts: a marker (e.g. radionuclide or fluorescent dye), a targeted binder (e.g. Affibody, antibody, or antibody fraction), and a linker. The parameters that have to be considered in designing a fluorescent probe (marker) are the emission and excitation wavelengths, quantum yield, stability, toxicity, and molecular size. The excitation wavelength determines the detection depth. Since absorption of tissue chromophore and water is lower in NIR region, fluorescent dyes in this spectral region have higher penetration depth in tissue than other wavelengths. The desire is to have minimal overlap of the emission and excitation spectrum. Fluorescent probes need to have high quantum yield to generate brighter fluorescence signal. The molecular size of the fluorescent probe is also important since it determines the pharmacokinetics and clearance time of the probe from the body. Using fluorescent probes that can turn on in specific conditions and turn off in other conditions can improve the image quality and signal to background ratio [152]. Fluorescence imaging has the potential to monitor multiple biomarkers simultaneously by using different fluorescent probes with different emission wavelengths [116, 153, 154]. In these applications, the excitation spectrum of each dye has to be narrow and as separate as possible. Multicolor imaging can be used to characterize several cancer biomarkers and/or to evaluate the effect of multiple drugs in vivo. It can also be used to study the pharmacokinetics of several drugs or probes with different clearance rates at the same time, which is unique among other imaging modalities.

As an alternative approach to fluorescence imaging, Wilson et al. [113, 116] have introduced phosphorescent probes for non-invasive monitoring of the hypoxic condition of tumors. Phosphorescent probes have longer temporal response (ms range) compared to fluorescent probes (ns). Due to its longer temporal response, the separation of the phosphorescence signal from excitation and autofluorescence signals (background noise) can be obtained by simple time gating. Also, implementation of a time-resolved phosphorescence imaging system is simpler and less expensive than a time-resolved fluorescence system.

As an example, in this section, we review the fluorescence imaging methods that have been developed by our group to detect and monitor specific cancer biomarker expression in vivo for diagnostics and therapy. Here we focus our study on the HER2 receptor, a cancer biomarker that is highly expressed in about 30% of breast cancer cases [155, 156]. Overexpression of this receptor is correlated with poor prognosis and resistance to specific chemotherapy [157]. To optimize the treatment procedure, it is important to identify the level of expression of the HER2 receptors during the diagnostic process and to monitor it over the course of treatment. Similar approaches can be used potentially for characterization of other disease or cancer-related biomarkers.

In clinical studies, the current diagnostic gold standards for detection of HER2 expressions are all based on ex vivo methods, such as immunohistochemistry (IHC), gene amplification based fluorescent in situ hybridization (FISH), and enzyme-linked immunosorbent assay (ELISA) [158]. These methods are invasive and require biopsies from the patients. Inherently, biopsies have a risk of missing the malignant lesion and, during the therapeutic cycle, the number of times that the biopsy can be taken is limited. The current goal is to replace these invasive methods with non-invasive imaging, reduce the time between imaging and diagnosis, and facilitate analysis of therapy progression in the clinic with portable and accessible systems.

In order to image the HER2 receptors, we used HER2-specific Affibody molecules as a targeting agent [159, 160]. Affibody molecules are highly water soluble, about 20 times smaller than antibodies, and 4 times smaller than antibody fragments [161, 162]. Due to their small size, they have better conjugation to HER2 receptors and shorter washout time from the body and normal tissues. To track these probes, Affibody molecules were conjugated to NIR fluorescent dyes. Affibody molecules were kindly provided by Affibody AB, Bromma, Sweden. Labeling of HER2-specific Affibody molecules with Alexa Fluor 750 fluorophores were described in detail by Lee et al. [160].
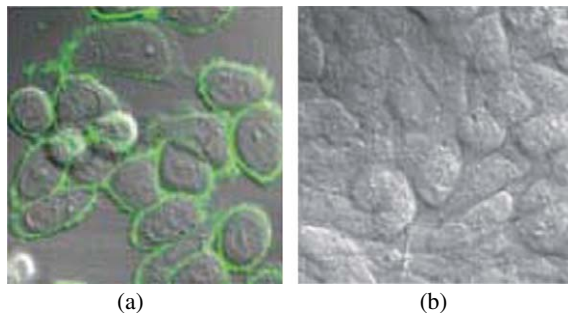
(a)   (b)

Fig. 7. Confocal microscopy studies show (a) binding of HER2-specific Affibody fluorescent probe with HER2 receptors in SKBR-3. (b) No binding was observed between HER2-specific Affibody fluorescent probe and U251 cells (after [160]).

Figure 7 shows the *in-vitro* experiments on Alexafluor 750-Affibody conjugate to study its selective binding to the HER2 receptors. In these experiments, the HER2-specific Affibody fluorescent probes were studied on SKBR-3 and U251 cell lines. SKBR-3 is a human breast adenocarcinoma cell line and has high expression of HER2 receptors. U251 is a human glioblastoma MG cell line and was selected as a non-expressing HER2 tumor model. After incubation of the cultured cells mixed with 1 nmol/L HER2-specific Affibody labeled with Alexafluor 750 at 37°C for one hour, cells were washed twice with media to remove the non-attached fluorophores and imaged by confocal fluorescence microscopy. Figure 7 shows binding of HER2-specific Affibody fluorescent probes on the surface of SKBR-3 cells which had high HER2 expression (Fig. 7a), however, they did not bind to U251 cells which did not have any HER2 expression (Fig. 7b).

The other important property of the HER2 Affibody is that it binds to a different epitope of the HER2 receptor than to the epitope targeted by monoclonal antibodies like trastuzumab or pertuzumab. This enables monitoring of HER2 expression during therapy without interference with the potential effect of these drugs [163]. The details of the *in-vitro* study to prove this are shown in Fig. 8.

In the first experiment, HER2-specific Affibody and trastuzumab molecules were labeled with different fluorophores. HER2-specific Affibody molecules were labeled with Alexafluor 488 (emission peak at 488 nm) and trastuzumab molecules were labeled with Alexafluor 630 (maximum emission at 630 nm). Tumor cells with high HER2 expression (SKBR-3) were mixed and incubated with both labeled HER2- specific Affibody and labeled trastuzumab. Since the emission wavelengths of Alexafluor 488 and Alexafluor 630 are different, different emission filters were used to separate their images. Figure 8a shows binding of both HER2-specific Affibody and trastuzumab molecules to the cells. In the next experiment, 100-fold excess unlabeled trastuzumab was added to the media to block the HER2 receptors.

After one-hour incubation, the labeled Affibody and labeled trastuzumab were added to the cell media and were incubated for one hour before imaging. Figure 8b shows that the unlabeled trastuzumab molecules completely blocked all the HER2 epitopes that could attach to labeled trastuzumab molecules. Therefore, from labeled trastuzumab and labeled Affibody experiments, only labeled Affibody molecules were bound to the cells confirming that the HER2 epitope that binds to HER2-specific Affibody molecule is different from the one that binds to trastuzumab.

The third experiment was the same as the second experiment, however, instead of unlabeled trastuzumab, we added 100-fold excess unlabeled HER2-specific Affibody to the cells. The results shown in Fig. 8c also confirm that the HER2 epitope that binds to HER2-specific Affibody molecule is different from the epitope that binds to trastuzumab. In the last experiment, 100-fold excess unlabeled HER2-specific Affibody and unlabeled trastuzumab were added to the cell media. After one hour incubation, labeled HER2-specific Affibody and labeled trastuzumab were added and incubated for one hour. The results in Fig. 8d shows that all HER2 epitopes were blocked with unlabeled Affibody and unlabeled trastuzumab; therefore, none of the labeled molecules could bind to HER2 receptors.

These *in-vitro* experiments were important to observe the toxicity and selective binding of the Affibody probe and its potential for imaging during therapy without any interference with treatment.

5.3. Fluorescence imaging algorithms

5.3.1. Fluorescent intensity imaging

Currently, most of the *in vivo* fluorescence studies are based on mapping fluorescence intensity. Figure 9 shows an example of the fluorescence intensity image of Dylight 750 Affibody conjugate probe *in vivo*.

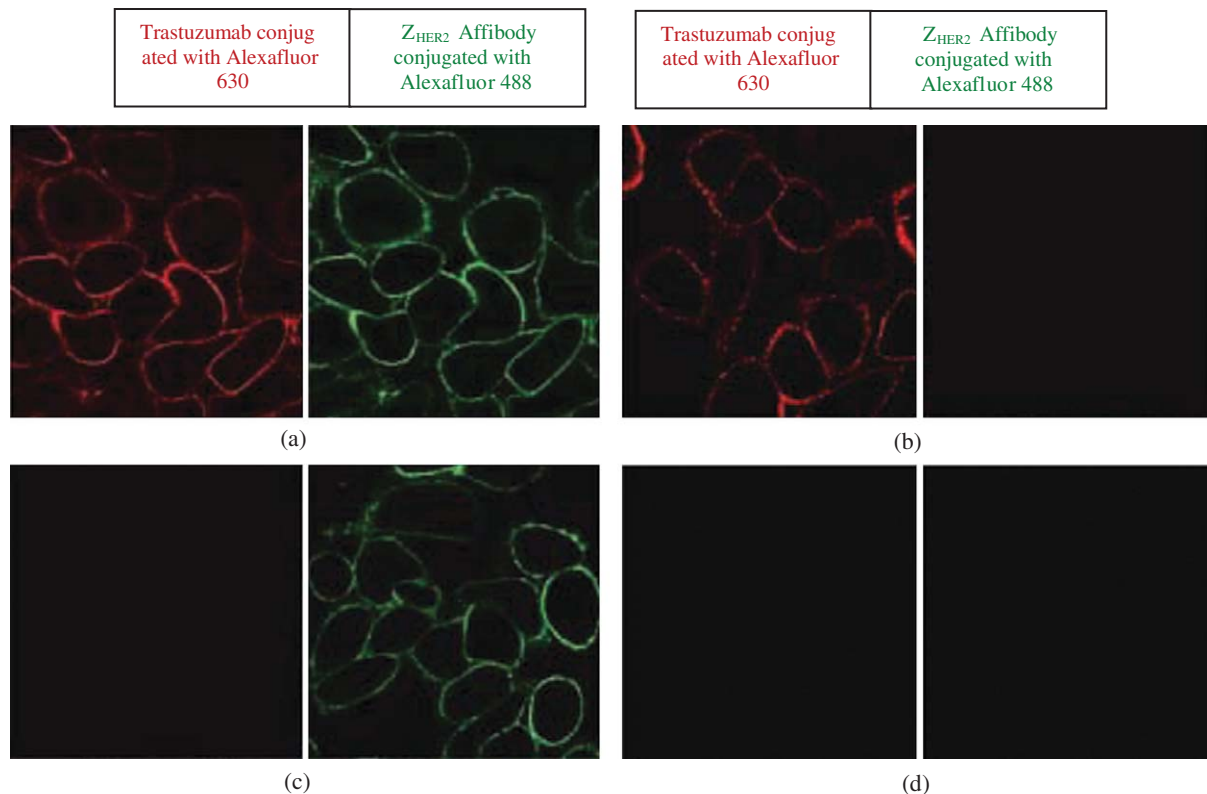In this experiment, BT474 and MDA-MB468 cell lines were used as high HER2- and no HER2-

Fig. 8. *In-vitro* study of binding Affibody (probe) and trastuzumab (MAB drug) to different epitopes of HER2 receptors. (a) Image of SKBR-3 cells after adding the labeled HER2-specific Affibody and labeled trastuzumab to the cell media. (b) Blocking HER2 epitopes with unlabeled 100-fold excess trastuzumab and image of the high HER2 expressing cancer cells after adding the labeled HER2-specific Affibody and labeled trastuzumab. (c) Blocking HER2 epitopes with unlabeled 100-fold excess HER2-specific Affibody molecules and image of the high HER2 expressing cancer cells after adding the labeled HER2-specific Affibody and labeled trastuzumab. (d) Blocking HER2 epitopes with unlabeled 100-fold excess HER2-specific Affibody molecules and unlabeled 100-fold excess trastuzumab and imaging the cells after adding the labeled HER2-specific Affibody and labeled trastuzumab (after [160]).

expressing human tumor models, respectively. The cells were implanted into the right forelimb of xenograft female nude mice. The study was approved by the National Institutes of Health Animal Safety and Use Committee. Five million cells were injected in 0.1 mL of 50% Matrigel into their right forelimb. The mice were imaged after the tumors grew to 0.5–1 cm in size and were anesthetized by Isoflurane before imaging. 10 μg of HER2-specific Affibody conjugated with Dylight 750 was injected in the mouse's tail vain. Figure 9 shows the fluorescence intensity of the tumor 3 hours after injection. As expected, the HER2-specific Affibody fluorescent probes bound to the HER2 receptors in the mouse tumor with BT474 tumor model and showed very high fluorescence intensity in the tumor region. However, the fluorescence intensity detected from MDA-MB468 tumor, which has no HER2 expression, is almost negligible.

The main drawback of using fluorescence intensity is its sensitivity to the fluctuations of the excitation light, distance of the probe from the tumor, and other parameters of the system.

Fluorescence tomography is being developed to characterize deeper tissue layers up to several centimeters. However, since the number of measurements is usually less than the number of reconstructed voxels, the inversion matrices that are involved in tomography reconstruction algorithms are ill-posed. In order to improve the quantitative values in the reconstructed image, the fluorescence imaging needs to be combined with a second imaging technique such as MRI, CT, or ultrasound [164]. More detailed reviews of
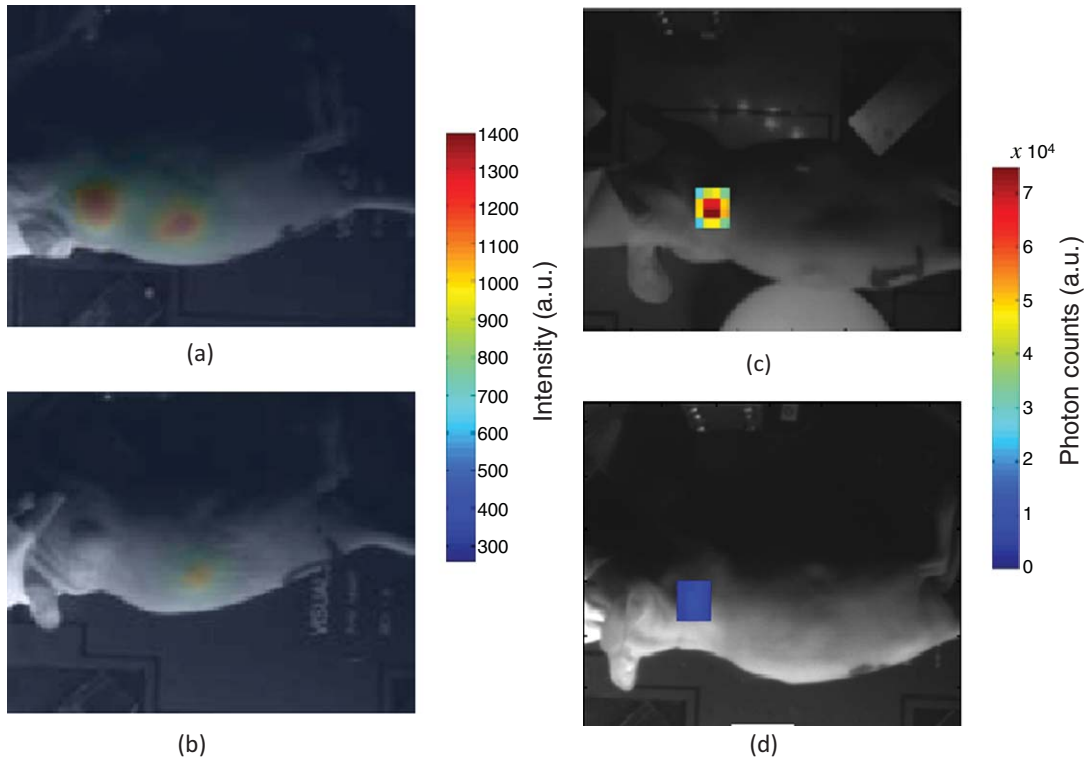
Fig. 9. *In-vivo* fluorescence intensity map of xenograft mouse with (a, c) high HER2-expressing human tumor model (BT474) and (b, d) no HER2-expressing human tumor model (MDA-MB468), 3 hours after injection of the HER2-specific Affibody® (His6-ZTaq-GS-Cys) conjugated to DyLight 750. Figures (a) and (b) were imaged by CW CCD camera, the data on figures c and d were captured by a time-resolved system.

these fluorescence imaging techniques can be found in references [110, 164, 165].

5.3.2. Quantitative estimation of cancer receptors in vivo

Even though the fluorescence intensity in tumors with high HER2-expressing tumor models is much higher than no HER2-expressing tumor models (Fig. 10a), using the fluorescence intensity information alone to quantify the HER2 receptors has some limitations.

Fluorescence intensity is very sensitive to the intensity variation of the excitation source, total blood volume in circulation, changes in system parameters, and concentration of the injected dye. To overcome this problem we introduced an algorithm based on the compartmental ligand-receptor model [166]. This algorithm uses the dynamic of the normalized fluorescence intensity (uptake) in the tumor compared to the normal tissues at the contralateral site [166].

The results were compared with ELISA, a standard *ex vivo* method that is commonly used to quantify cancer biomarkers.

Considering that the dissociation rate of bound fluorophores is very low, the fluorescence intensity can be written as

$$
\begin{aligned}
I_f &= I_{free\ ligands\ in\ blood} + I_{free\ ligands\ in\ the\ tumor} \\
&\quad + I_{bound\ ligand-receptor} = \alpha F_{b1} \exp\left(-\frac{t}{\tau}\right) \\
&\quad + \beta F_T + \gamma B_{\max}\left[1 - \exp\left(-k_{on}\, t F_T\right)\right] \quad (5)
\end{aligned}
$$

where α, β, *and* γ are constants, F_{bl}, F_T and B_{max} are the number of free ligands in the blood, and free and bound ligands to the receptors in the tumor region, respectively, τ is the time constant of the clearance of the fluorophores from the normal tissue, and k_{on} is the kinetics rate of ligand-receptor binding. In this approximation, we assumed that after the initial time t_1, the concentration of local free ligands in tumor stays constant. The intensity of the free ligands in blood can
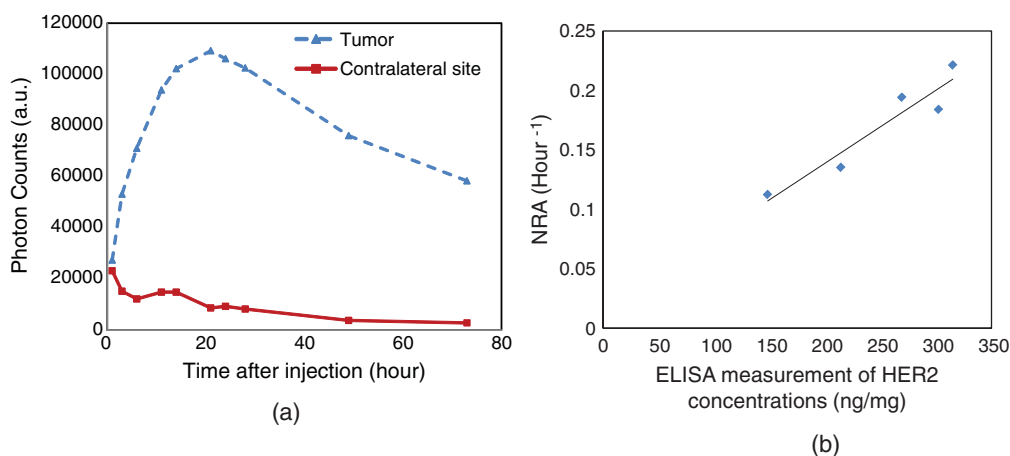
Fig. 10. (a) *In vivo* measurements of optical intensity at the tumor and contralateral sites over time (BT474 tumor) after injection of ABD-(Z$_{HER2:342}$)$_2$ Affibody labeled with Alexafluor 750 (b) Estimated NRA of several BT474 tumors with different HER2 expression vs. *ex vivo* measurement of HER2 concentration obtained by ELISA assay (after [166]).

be considered as the same as the intensity measured at the contralateral site. Therefore, if we subtract the measurements at the contralateral site from the tumor site, the two remaining components will be the free and bound ligands to the receptors in the tumor region, which can be simplified as

$$y(t) = y_0 + a[1 - \exp(-bt)] \tag{6}$$

To eliminate the system variations between different experiments, we normalized the measurement data at different time points to the first measurement data, when binding was almost negligible and the accumulation of the free ligands in the tumor was stabilized.

The derivative $\left.\frac{dy}{dt}\right|_{t=0} = ab$ presents the normalized rate of accumulation (NRA). By using a fitting algorithm, NRA can be estimated from a time series of fluorescence intensity measurements. To confirm our results, we compared the estimated NRA of several BT474 tumors with different HER2 expression by the values obtained *ex vivo* for the same tumor by ELISA assay (Fig. 10b). The results show a good linear correlation between the NRA and HER2 concentration obtain by ELISA [166]. The ELISA assay was performed according to the protocol provided by the manufacturer (Calbiochem, Gibbstown, NJ) and HER2 concentration is expressed in nanograms of HER2 per milligram of total protein.

5.3.3. Fluorescence lifetime imaging

The other measurable parameter in fluorescence imaging is the fluorescence lifetime. In the frequency domain method, based on amplitude and phase measurements, two fluorescence lifetimes can be defined: phase lifetime (τ_p) and modulation lifetime (τ_M). The definitions of these two lifetimes are as follows,

$$\tau_p = \frac{\tan(\varphi)}{\omega}; \ \tau_M = \left(\frac{1}{\omega}\right) \sqrt{\left(\frac{1}{M^2} - 1\right)} \tag{7}$$

where φ is the phase shift, ω is the angular modulation frequency of the excitation light, and M is the attenuation in modulation depth of the received signal [167].

If the media contains only one kind of fluorophore, the phase and modulation lifetime will be equal. However, if the medium contains different fluorophores, then the value of these two parameters can be different and can be used to distinguish and separate the images of each fluorophore.

To calculate the fluorescence lifetime using the time domain method [168], the measured signal can be written as:

$$I(t) = IRF \otimes I_0 e^{-t/\tau} \tag{8}$$

where IRF is the impulse response function of the system, $\otimes$ is the convolution, I_0 is the intensity of the excitation light, and τ is the fluorescence lifetime. The fluorescence lifetime can be estimated by curve fitting methods, such as a least-squares algorithm. If the

medium contains more than one kind of fluorophore, a multi-exponential curve-fitting algorithm needs to be applied.

Equations (7) and (8) are valid if the effects of photon migration on the apparent fluorescence lifetime τ' (determined as an observed exponential decay time of emission intensity I(t)) are negligible. If the fluorophore is embedded deeper than several scattering lengths $l_s \sim 1/\mu_s'$ in the turbid medium (μ_s' is the transport-corrected scattering coefficient), measured values of τ' are larger than intrinsic fluorescence lifetime τ. Time-resolved fluorescence intensity distribution presents the convolution of the exponential decay curve, similar to Equation (6), and Green functions, describing photon migration from the source to the fluorophore inside the turbid medium and from the fluorophore to the detector [169, 170].

6. Summary

In this Chapter, a general overview of existing *in-vivo* optical imaging techniques was given. The rapid progress of the field over the past few decades clearly demonstrates its capability for use in several medical applications, including cancer and functional brain imaging. In cancer imaging, diffuse optical tomography measures the differences between the optical signature of cancer lesions and normal tissues. In functional brain imaging, near infrared spectroscopy has been widely used to measure cerebral hemodynamic changes in various parts of the cortex. Furthermore, it has been shown that NIRS can capture fast optical scattering changes, making it the only neuroimaging tool that is capable of measuring both hemodynamic and neuronal signals simultaneously. In fluorescent imaging, targeted fluorescent probes are expected to potentially create new imaging and treatment paradigms in cancer diagnostics and therapy.

Acknowledgments

References

[1] M. Cutler, Transillumination of the Breast, *Ann Surg* **93** (1931), 223–234.

[2] F.F. Jobsis, Noninvasive, infrared monitoring of cerebral and myocardial oxygen sufficiency and circulatory parameters, *Science* **198** (1977), 1264–1267.

[3] M.S. Patterson et al., Time resolved reflectance and transmittance for the non-invasive measurement of tissue optical properties, *Appl Opt* **28** (1989), 2331–2336.

[4] G. Strangman et al., Non-invasive neuroimaging using near-infrared light, *Biological Psychiatry* **52** (2002), 679–693.

[5] A.E. Cerussi et al., Sources of absorption and scattering contrast for near-infrared optical mammography, *Academic Radiology* **8** (2001), 211–218.

[6] T. Durduran et al., Bulk optical properties of healthy female breast tissue, *Physics in Medicine and Biology* **47** (2002), 2847–2861.

[7] S. Kukretia et al., Intrinsic near-infrared spectroscopic markers of breast tumors, *Disease Markers* **25** (2008), 281–290.

[8] A. Gibson et al., Recent advances in diffuse optical imaging, *Physics in Medicine and Biology* **50** (2005), R1.

[9] R.D. Frostig, *In vivo* optical imaging of brain function, *CRC*, 2002.

[10] E.M.C. Hillman, Optical brain imaging *in vivo*: Techniques and applications from animal to man, *Journal of Biomedical Optics* **12** (2007), 051402.

[11] B. Bonakdarpour et al., Hemodynamic response function in patients with stroke-induced aphasia: Implications for fMRI data analysis, *Neuroimage* **36** (2007), 322–331.

[12] J. Steinbrink et al., Determining changes in NIR absorption using a layered model of the human head, *Physics in Medicine and Biology* **46** (2001), 879.

[13] S.R. Arridge, Optical tomography in medical imaging, *Inverse Problems* **15** (1999), R41–R93.

[14] H. Kawaguchi et al., Theoretical evaluation of accuracy in position and size of brain activity obtained by near-infrared topography, *Physics in Medicine and Biology* **49** (2004), 2753.

[15] T. Austin et al., Three dimensional optical imaging of blood volume and oxygenation in the neonatal brain, *Neuroimage* **31** (2006), 1426–1433.

[16] G. Gulsen et al., Combined diffuse optical tomography (DOT) and MRI system for cancer imaging in small animals, *Technology in Cancer Research & Treatment* **5** (2006), 351–363.

[17] Q. Zhang et al., Coregistered tomographic x-ray and optical breast imaging: Initial results, *Journal of Biomedical Optics* **10** (2005), 024033:1–9.

[18] B. Brooksby et al., Imaging breast adipose, fibroglandular tissue molecular signatures by using hybrid MRI-guided near-infrared spectral, tomography, *Proceedings of the National Academy of Sciences of the United States of America* **103** (2006), 8828–8833.

[19] V. Ntziachristos et al., MRI-guided diffuse optical spectroscopy of malignant and benign breast lesions, *Neoplasia* **4** (2002), 347–354.

[20] Q.I. Zhu et al., Ultrasound-guided optical tomographic imaging of malignant and benign breast lesions: Initial clinical results of 19 cases, *Neoplasia* **5** (2003), 379–388.

[21] S.R. Arridge, Photon-measurement density functions. Part I: Analytical forms, *Applied Optics* **34** (1995), 7395–7409.

[22] S.R. Arridge and M. Schweiger, Photon-measurement density functions. Part 2: Finite-element-method calculations, *Applied Optics* **34** (1995), 8026–8037.

[23] H. Dehghani et al., Near infrared optical tomography using NIRFAST: Algorithm for numerical model and image reconstruction, *Communications in Numerical Methods in Engineering* **25** (2009), 711–732.

[24] S. Srinivasan et al., A boundary element approach for image-guided near-infrared absorption and scatter estimation, *Medical Physics* **34** (2007), 4545–4557.

[25] S.R. Arridge and M. Schweiger, Image reconstruction in optical tomography, *Philosophical Transactions of the Royal Society B-Biological Sciences* **352** (1997), 717–726.

[26] L.H. Wang et al., MCML - Monte-carlo modeling of light transport in multilayered tissues light transport in multilayered tissues, *Computer Methods and Programs in Biomedicine* **47** (1995), 131–146.

[27] S.R. Arridge and J.C. Schotland, Optical tomography: Forward and inverse problems, *Inverse Problems* **25** (2009).

[28] D.A. Boas et al., Imaging the body with diffuse optical tomography, *IEEE Signal Processing Magazine* **18** (2001), 57–75.

[29] G.F. Knoll, *Radiation detection and measurement*, Wiley 2010.

[30] S.R. Arridge and W.R.B. Lionheart, Nonuniqueness in diffusion-based optical tomography, *Optics Letters* **23** (1998), 882–884.

[31] A. Corlu et al., Diffuse optical tomography with spectral constraints and wavelength optimization, *Applied Optics* **44** (2005), 2082–2093.

[32] D.J. Cuccia et al., Modulated imaging: Quantitative analysis and tomography of turbid media in the spatial-frequency domain, *Optics Letters* **30** (2005), 1354–1356.

[33] S.D. Konecky et al., Quantitative optical tomography of subsurface heterogeneities using spatially modulated structured light, *Optics Express* **17** (2009), 14780–14790.

[34] C.H. Schmitz et al., Instrumentation for fast functional optical tomography, *Review of Scientific Instruments* **73** (2002), 429–439.

[35] G. Gratton et al., Fast and localized event-related optical signals (EROS) in the human occipital cortex: Comparisons with the visual evoked potential and fMRI, *Neuroimage* **6** (1997), 168–180.

[36] S.L. Jacques and B.W. Pogue, Tutorial on diffuse light transport, *Journal of Biomedical Optics* **13** (2008), 041302:1–19.

[37] S.R. Arridge et al., The theoretical basis for the determination of optical pathlengths in tissue - temporal and frequency-analysis, *Physics in Medicine and Biology* **37** (1992), 1531–1560.

[38] R. Nachabe et al., Estimation of lipid and water concentrations in scattering media with diffuse optical spectroscopy from 900 to 1,600 nm, *Journal of Biomedical Optics* **15** (2010), 037015.

[39] A. Cerussi et al., Predicting response to breast cancer neoadjuvant chemotherapy using diffuse optical spectroscopy, *Proceedings of the National Academy of Sciences of the United States of America* **104** (2007), 4014–4019.

[40] R. Choe et al., Diffuse optical tomography of breast cancer during neoadjuvant chemotherapy: A case study

[41] with comparison to MRI, *Medical Physics* **32** (2005), 1128–1139.

[41] V. Ntziachristos et al., Concurrent MRI and diffuse optical tomography of breast after indocyanine green enhancement, *Proceedings of the National Academy of Sciences of the United States of America* **97** (2000), 2767–2772.

[42] E.M. Hillman, Optical brain imaging *in vivo*: Techniques and applications from animal to man, *Journal of Biomedical Optics* **12** (2007), 051402.

[43] X. Cui et al., A quantitative comparison of NIRS and fMRI across multiple cognitive tasks, *Neuroimage* **54** (2011), 2808–2821.

[44] I.L. Kwee and T. Nakada, Dorsolateral prefrontal lobe activation declines significantly with age–functional NIRS study, *J Neurol* **250** (2003), 525–529.

[45] K. Izzetoglu et al., Functional optical brain imaging using near-infrared during cognitive tasks, *International Journal of Human-Computer Interaction* **17** (2004), 211–227.

[46] A. Villringer and B. Chance, Non-invasive optical spectroscopy and imaging of human brain function, *Trends Neurosci* **20** (1997), 435–442.

[47] T. Suto et al., Multichannel near-infrared spectroscopy in depression and schizophrenia: Cognitive brain activation study, *Biol Psychiatry* **55** (2004), 501–511.

[48] S.J. Gilbert et al., Functional specialization within rostral prefrontal cortex (area 10): A meta-analysis, *J Cogn Neurosci* **18** (2006), 932–948.

[49] M.J. Herrmann et al., Cerebral oxygenation changes in the prefrontal cortex: Effects of age and gender, *Neurobiol Aging* **27** (2006), 888–894.

[50] G.M. Lech, Using functional near-infrared spectroscopy to measure cognitive function: When will it become an accepted clinical tool for cognitive aging and prodromal dementia screening? *Journal of Innovative Optical Health Sciences* **4** (2011), 373–383.

[51] C. Li et al., Verbal working memory load affects prefrontal cortices activation: Evidence from a functional NIRS study in humans, Progress in Biomedical Optics and Imaging - Proceedings of SPIE **5696** (2005), 33–40.

[52] D. Bastien et al., Specific functional asymmetries of the human visual cortex revealed by functional Near-Infrared Spectroscopy, *Brain Research* **1431** (2011), 62–68.

[53] L. Perkins, The use of Near Infrared Spectroscopy in measuring haemodynamic response of the primary visual cortex to a visual bullseye stimulus with various spatial and temporal frequencies, *The Plymouth Student Scientist* **4** (2011), 131–154.

[54] T. Kato et al., Human visual cortical function during photic stimulation monitoring by means of near-infrared spectroscopy, *Journal of Cerebral Blood Flow and Metabolism* **13** (1993), 516–516.

[55] K. Takahashi et al., Activation of the visual cortex imaged by 24-channel near-infrared spectroscopy, *Journal of Biomedical Optics* **5** (2000), 93.

[56] M. Plichta et al., Model-based analysis of rapid event-related functional near-infrared spectroscopy (NIRS) data: A parametric validation study, *Neuroimage* **35** (2007), 625–634.

[57] V.Y. Toronov et al., A spatial and temporal comparison of hemodynamic signals measured using optical and functional

magnetic resonance imaging during activation in the human primary visual cortex, *Neuroimage* **34** (2007), 1136–1148.

[58] M.A. McIntosh et al., Absolute Quantification of Oxygenated Hemoglobin within the Visual Cortex with Functional Near Infrared Spectroscopy (fNIRS), *Investigative Ophthalmology & Visual Science* **51** (2010), 4856–4860.

[59] L. Minati et al., Variability comparison of simultaneous brain near-infrared spectroscopy (NIRS) and functional MRI (fMRI) during visual stimulation, *Journal of Medical Engineering & Technology* **35** (2011), 370.

[60] M. Lassonde et al., Specific functional asymmetries of the human visual cortex revealed by functional Near-Infrared Spectroscopy, *Journal of Vision* **11** (2011), 1068–1068.

[61] D.R. Leff et al., Assessment of the cerebral cortex during motor task behaviours in adults: A systematic review of functional near infrared spectroscopy (fNIRS) studies, *Neuroimage* **54** (2011), 2922–2936.

[62] L. Gagnon et al., Quantification of the cortical contribution to the NIRS signal over the motor cortex using concurrent NIRS-fMRI measurements, *Neuroimage* **59** (2011), 3933–3940.

[63] T. Kusaka et al., Functional lateralization of sensorimotor cortex in infants measured using multichannel near-infrared spectroscopy, *Pediatric Research* **69** (2011), 430.

[64] C. Hirth et al., Non-invasive functional mapping of the human motor cortex using near-infrared spectroscopy, *Neuroreport* **7** (1996), 1977.

[65] W. Colier et al., Human motor-cortex oxygenation changes induced by cyclic coupled movements of hand and foot, *Experimental Brain Research* **129** (1999), 457–461.

[66] Y. Murata et al., Decreases of blood oxygenation level—dependent signal in the activated motor cortex during functional recovery after resection of a glioma, *American Journal of Neuroradiology* **25** (2004), 1242–1246.

[67] D. Leamy et al., Combining fNIRS and EEG to improve motor cortex activity classification during an imagined movement-based task, *Foundations of Augmented Cognition. Directing the Future of Adaptive Systems* (2011), 177–185.

[68] M. Shibusawa et al., Functional near-infrared spectroscopy study on primary motor and sensory cortex response to clenching, *Neuroscience Letters* **449** (2009), 98–102.

[69] B. Khan et al., Identification of abnormal motor cortex activation patterns in children with cerebral palsy by functional near-infrared spectroscopy, *Journal of Biomedical Optics* **15** (2010), 036008.

[70] K. Sakatani et al., Language-activated cerebral blood oxygenation and hemodynamic changes of the left prefrontal cortex in poststroke aphasic patients: A near-infrared spectroscopy study, *Stroke* **29** (1998), 1299–1304.

[71] I. Kovelman et al., Dual language use in sign-speech bimodal bilinguals: fNIRS brain-imaging evidence, *Brain and Language* **109** (2009), 112–123.

[72] L. Sugiura et al., Sound to language: Different cortical processing for first and second languages in elementary school children as revealed by a large-scale study using fNIRS, *Cerebral Cortex* **21** (2011), 2374–2393.

[73] A. Gallagher et al., The contribution of functional near-infrared spectroscopy (fNIRS) to the presurgical assessment

of language function in children, *Brain and Language* (2011), in press.

[74] M.H. Dubins, *An investigation of early phonetic processing in monolingual and bilingual infants using new functional Near-Infrared Spectroscopy (fNIRS)*, University of Toronto, 2010.

[75] S. Benavides-Varela et al., Studying neonates' language and memory capacities with functional near-infrared spectroscopy, *Frontiers in Psychology* **2** (2011), 64.

[76] S. Rossi et al., Shedding light on words and sentences: Near-infrared spectroscopy in language research, *Brain and language* (2011), in press.

[77] Y. Hoshi et al., Interpretation of near-infrared spectroscopy signals: A study with a newly developed perfused rat brain model, *Journal of Applied Physiology* **90** (2001), 1657.

[78] H. Obrig et al., Cerebral oxygenation changes in response to motor stimulation, *Journal of Applied Physiology* **81** (1996), 1174–1183.

[79] S.A. Huettel et al., *Functional Magnetic Resonance Imaging*, Sinauer Associates Sunderland, MA, 2004.

[80] M. Kohl et al., Physical model for the spectroscopic analysis of cortical intrinsic optical signals, *Physics in Medicine and Biology* **45** (2000), 3749.

[81] T.J. Huppert et al., HomER: A review of time-series analysis methods for near-infrared spectroscopy of the brain, *Applied Optics* **48** (2009), D280–D298.

[82] A. Ishimaru, *Wave propagation and scattering in random media*, Wiley-IEEE Press, 1999.

[83] M.S. Patterson et al., Time resolved reflectance and transmittance for the non-invasive measurement of tissue optical properties, *Applied Optics* **28** (1989), 2331–2336.

[84] R.C. Haskell et al., Boundary conditions for the diffusion equation in radiative transfer, *JOSA A* **11** (1994), 2727–2741.

[85] D.A. Boas et al., Diffuse optical imaging of brain activation: Approaches to optimizing image sensitivity, resolution, and accuracy, *Neuroimage* **23** (2004), S275–S288.

[86] F. Robertson et al., Motion artifact removal for functional near infrared spectroscopy: A comparison of methods, *Biomedical Engineering, IEEE Transactions on* **57** (2010), 1377–1387.

[87] I. Miyai et al., Cortical mapping of gait in humans: A near-infrared spectroscopic topography study, *Neuroimage* **14** (2001), 1186–1192.

[88] M. Izzetoglu et al., Motion artifact cancellation in NIR spectroscopy using Wiener filtering, *Biomedical Engineering, IEEE Transactions on* **52** (2005), 934–938.

[89] T. Wilcox et al., Using near-infrared spectroscopy to assess neural activation during object processing in infants, *Journal of Biomedical Optics* **10** (2005), 011010.

[90] R. Sitaram et al., Temporal classification of multichannel near-infrared spectroscopy signals of motor imagery for developing a brain-computer interface, *Neuroimage* **34** (2007), 1416–1427.

[91] L. Becerra et al., Diffuse optical tomography of pain and tactile stimulation: Activation in cortical sensory and emotional systems, *Neuroimage* **41** (2008), 252–259.

[92] H. Sato et al., Wavelet analysis for detecting body-movement artifacts in optical topography signals, *Neuroimage* **33** (2006), 580–587.

[93] M.A. Franceschini et al., Diffuse optical imaging of the whole head, *Journal of Biomedical Optics* **11** (2006), 054007.

[94] Y. Zhang et al., Eigenvector-based spatial filtering for reduction of physiological interference in diffuse optical imaging, *Journal of Biomedical Optics* **10** (2005), 011014.

[95] J. Steinbrink et al., Somatosensory evoked fast optical intensity changes detected non-invasively in the adult human head, *Neuroscience Letters* **291** (2000), 105–108.

[96] J. Steinbrink et al., The fast optical signal–robust or elusive when non-invasively measured in the human adult? *Neuroimage* **26** (2005), 996–1008.

[97] R. Stepnoski et al., Noninvasive detection of changes in membrane potential in cultured neurons by light scattering, *Proceedings of the National Academy of Sciences* **88** (1991), 9382.

[98] G. Gratton and M. Fabiani, Fast optical imaging of human brain function, *Frontiers in Human Neuroscience* **4** (2010), 52.

[99] G. Gratton et al., Memory-driven processing in human medial occipital cortex: An event-related optical signal (EROS) study, *Psychophysiology* **35** (1998), 348–351.

[100] E.L. Maclin et al., Optimum filtering for EROS measurements, *Psychophysiology* **40** (2003), 542–547.

[101] E.L. Maclin et al., The event-related optical signal to electrical stimulation of the median nerve, *Neuroimage* **21** (2004), 1798–1804.

[102] M.A. Franceschini and D.A. Boas, Noninvasive measurement of neuronal activity with near-infrared optical imaging, *Neuroimage* **21** (2004), 372–386.

[103] A.V. Medvedev et al., Event-related fast optical signal in a rapid object recognition task: Improving detection by the independent component analysis, *Brain Research* **1236** (2008), 145–158.

[104] K.A. Low et al., Fast optical imaging of frontal cortex during active and passive oddball tasks, *Psychophysiology* **43** (2006), 127–136.

[105] G. Morren et al., Detection of fast neuronal signals in the motor cortex from functional near infrared spectroscopy measurements using independent component analysis, *Medical and Biological Engineering and Computing* **42** (2004), 92–99.

[106] A. Medvedev et al., *Fast optical signal in the prefrontal cortex correlates with EEG*, Springer, 2010.

[107] M. Wolf et al., Fast cerebral functional signal in the 100-ms range detected in the visual cortex by frequency-domain near-infrared spectrophotometry, *Psychophysiology* **40** (2003), 521–528.

[108] L. Cohen and R. Keynes, Changes in light scattering associated with the action potential in crab nerves, *The Journal of Physiology* **212** (1971), 259.

[109] M. Monici, Cell and tissue autofluorescence research and diagnostic applications, *Biotechnol Annu Rev* **11** (2005), 227–256.

[110] V. Ntziachristos, Fluorescence molecular imaging, *Annu Rev Biomed Eng* **8** (2006), 1–33.

[111] A. Soubret et al., Accuracy of fluorescent tomography in the presence of heterogeneities: Study of the normalized born ratio, *IEEE Trans Med Imaging* **24** (2005), 1377–1386.

[112] G. Themelis et al., Real-time intraoperative fluorescence imaging system using light-absorption correction, *Journal of Biomedical Optics* **14** (2009), 064012.

[113] S.V. Apreleva et al., Tomographic imaging of oxygen by phosphorescence lifetime, *Appl Opt* **45** (2006), 8547–8559.

[114] S.C. Davis et al., Magnetic resonance-coupled fluorescence tomography scanner for molecular imaging of tissue, *Review of Scientific Instruments* **79** (2008), 064302.

[115] J.D. Gruber et al., System development for high frequency ultrasound-guided fluorescence quantification of skin layers, *Journal of Biomedical Optics* **15** (2010), 026028.

[116] A.Y. Lebedev et al., Dendritic phosphorescent probes for oxygen imaging in biological systems, *ACS Appl Mater Interfaces* **1** (2009), 1292–304.

[117] M. Nahrendorf et al., Hybrid PET-optical imaging using targeted probes, *Proc Natl Acad Sci U S A* **107** (2010), 7910–7915.

[118] D. Razansky and V. Ntziachristos, Hybrid photoacoustic fluorescence molecular tomography using finite-element-based inversion, *Medical Physics* **34** (2007), 4293–4301.

[119] L. Sampath et al., Detection of cancer metastases with a dual-labeled near-infrared/positron emission tomography imaging agent, *Transl Oncol* **3** (2010), 307–217.

[120] R.B. Schulz et al., Hybrid system for simultaneous fluorescence and x-ray computed tomography, *IEEE Trans Med Imaging* **29** (2010), 465–473.

[121] D. Thayer et al., Dual-Contrast Dynamic MRI-DOT for small animal imaging, *Technology in Cancer Research & Treatment* **9** (2010), 61–69.

[122] Y. Tan and H. Jiang, DOT guided fluorescence molecular tomography of arbitrarily shaped objects, *Medical Physics* **35** (2008), 5703–5707.

[123] Y. Lin et al., Fluorescence diffuse optical tomography with functional and anatomical a priori information: Feasibility study, *Physics in Medicine and Biology* **52** (2007), 5569–5585.

[124] M. Hassan et al., Fluorescence lifetime imaging system for *in vivo* studies, *Mol Imaging* **6** (2007), 229–236.

[125] A. Bassi et al., Time-gated optical projection tomography, *Optics Letters* **35** (2010), 2732–2734.

[126] A. Godavarty et al., Three-dimensional fluorescence lifetime tomography, *Medical Physics* **32** (2005), 992–1000.

[127] R.E. Nothdurft et al., *In vivo* fluorescence lifetime tomography, *Journal of Biomedical Optics* **14** (2009), 024004.

[128] M.A. OLeary et al., Fluorescence lifetime imaging in turbid media, *Optics Letters* **21** (1996), 158–160.

[129] J. Riley et al., Choice of data types in time resolved fluorescence enhanced diffuse optical tomography, *Medical Physics* **34** (2007), 4890–4900.

[130] M.Y. Berezin and S. Achilefu, Fluorescence lifetime measurements and biological imaging, *Chemical Reviews* **110** (2010), 2641–2684.

[131] H. Szmacinski and J.R. Lakiwicz, *Topics in Fluorescence Spectroscopy. Lifetime-based Sensing*, Plenum, New York, 1994.

[132] J.R. Lakowicz, *Principles of fluorescence spectroscopy*, Kluwer Academic/Plenum, New York, 1999.

[133] S. Bloch et al., Whole-body fluorescence lifetime imaging of a tumor-targeted near-infrared molecular probe in mice, *Journal of Biomedical Optics* **10** (2005), 054003.

[134] I. Gannot et al., Functional optical detection based on pH dependent fluorescence lifetime, *Lasers Surg Med* **35** (2004), 342–348.

[135] J.R. Griffiths, Are cancer cells acidic? *Br J Cancer* **64** (1991), 425–427.

[136] R. Nahta and F.J. Esteva, Herceptin: Mechanisms of action and resistance, *Cancer Lett* **232** (2006), 123–138.

[137] R. Richards-Kortum and E. Sevick-Muraca, Quantitative optical spectroscopy for tissue diagnosis, *Annu Rev Phys Chem* **47** (1996), 555–606.

[138] B. Zawirska, Comparative, porphyrin content in tumors with contiguous non-neoplastic tissues, *Neoplasma* **26** (1979), 223–229.

[139] G.A. Wagnieres et al., *In vivo* fluorescence spectroscopy and imaging for oncological applications, *Photochemistry and Photobiology* **68** (1998), 603–632.

[140] S.G. Demos et al., Spectroscopic detection of bladder cancer using near-infrared imaging techniques, *Journal of Biomedical Optics* **9** (2004), 767–771.

[141] D. Ramsoekh et al., A back-to-back comparison of white light video endoscopy with autofluorescence endoscopy for adenoma detection in high-risk subjects, *Gut* **59** (2010), 785–793.

[142] A. Becker et al., Receptor-targeted optical imaging of tumors with near-infrared fluorescent ligands, *Nature Biotechnology* **19** (2001), 327–331.

[143] S. Kizaka-Kondoh et al., Tumor hypoxia: A target for selective cancer therapy, *Cancer Science* **94** (2003), 1021–1028.

[144] M.Y. Berezin et al., Near-Infrared Fluorescence Lifetime pH-Sensitive Probes, *Biophysical Journal* **100** (2011), 2063–2072.

[145] T. Ueno and T. Nagano, Fluorescent probes for sensing and imaging, *Nat Methods* **8** (2011), 642–645.

[146] A. Corlu et al., Three-dimensional *in vivo* fluorescence diffuse optical tomography of breast cancer in humans, *Optics Express* **15** (2007), 6696–6716.

[147] Y. Ardeshirpour et al., Using *in-vivo* fluorescence imaging in personalized cancer diagnostics and therapy, an image and treat paradigm, *Technol Cancer Res Treat* **10** (2011), 549–560.

[148] G.P. Adams and L.M. Weiner, Monoclonal antibody therapy of cancer, *Nature Biotechnology* **23** (2005), 1147–1157.

[149] A.L. Nelson et al., Development trends for human monoclonal antibody therapeutics, *Nature Reviews Drug Discovery* **9** (2010), 767–774.

[150] J.M. Reichert, Antibodies to watch in 2010, *Mabs* **2** (2010), 84–100.

[151] G.J. Kelloff et al., The progress and promise of molecular imaging probes in oncologic drug development, *Clinical Cancer Research* **11** (2005), 7967–7985.

[152] H. Kobayashi et al., New strategies for fluorescent probe design in medical diagnostic imaging, *Chemical Reviews* **110** (2010), 2620–2640.

[153] J.V. Frangioni, *In vivo* near-infrared fluorescence imaging, *Curr Opin Chem Biol* **7** (2003), 626–634.

[154] D. Thayer et al., Dual-contrast dynamic MRI-DOT for small animal imaging, *Technol Cancer Res Treat* **9** (2010), 61–70.

[155] D.J. Slamon et al., Human breast cancer: Correlation of relapse and survival with amplification of the HER-2/neu oncogene, *Science* **235** (1987), 177–182.

[156] J. Zidan et al., Comparison of HER-2 overexpression in primary breast cancer and metastatic sites and its effect on biological targeting therapy of metastatic disease, *Br J Cancer* **93** (2005), 552–556.

[157] S. Menard et al., Biologic and therapeutic role of HER2 in cancer, *Oncogene* **22** (2003), 6570–6578.

[158] C.B. Moelans et al., Current technologies for HER2 testing in breast cancer, *Crit Rev Oncol Hematol* **8** (2011), 380–392.

[159] J. Capala and K. Bouchelouche, Molecular imaging of HER2-positive breast cancer: A step toward an individualized 'image and treat' strategy, *Curr Opin Oncol* **22** (2010), 559–566.

[160] S.B. Lee et al., Affibody molecules for *in vivo* characterization of HER2-positive tumors by near-infrared imaging, *Clinical Cancer Research* **14** (2008), 3840–3849.

[161] J. Lofblom et al., Affibody molecules: Engineered proteins for therapeutic, diagnostic and biotechnological applications, *FEBS Lett* **584** (2010), 2670–2680.

[162] V. Tolmachev et al., Affibody molecules: Potential for *in vivo* imaging of molecular targets for cancer therapy, *Expert Opin Biol Ther* **7** (2007), 555–568.

[163] J. Capala et al., Affibody molecules for *in vivo* characterization of HER2-positive tumors by near-infrared imaging, *Clinical Cancer Research* **14** (2008), 3840–3849.

[164] F. Leblond et al., Pre-clinical whole-body fluorescence imaging: Review of instruments, methods and applications, *J Photochem Photobiol B* **98** (2010), 77–94.

[165] K.W. Dunn and T.A. Sutton, Functional studies in living animals using multiphoton microscopy, *ILAR J* **49** (2008), 66–77.

[166] V. Chernomordik et al., Quantitative analysis of Her2 receptor expression *in vivo* by near-infrared optical imaging, *Mol Imaging* **9** (2010), 192–200.

[167] Y. Chen and R.M. Clegg, Fluorescence lifetime-resolved imaging, *Photosynth Res* **102** (2009), 143–155.

[168] W. Becker, *Advanced time-correlated single photon counting techniques*, Springer, Berlin, New York, 2005.

[169] V. Chernomordik et al., A CTRW-based model of time-resolved fluorescence lifetime imaging in a turbid medium, *Optics Communications* **283** (2010), 4832–4839.

[170] S.H. Han et al., Analytical method for the fast time-domain reconstruction of fluorescent inclusions *in vitro* and *in vivo*, *Biophysical Journal* **98** (2010), 350–357.